

3D Non-Stationary GBSMs for High-Speed Train Tunnel Channels

Yu Liu¹, Liu Feng², Jian Sun¹, Wensheng Zhang¹, Cheng-Xiang Wang³, Pingzhi Fan²

¹Shandong Provincial Key Lab of Wireless Communication Technologies, Shandong University, Jinan, Shandong, China

²Institute of Mobile Communications, Southwest Jiaotong University, Chengdu, China

³Institute of Sensors, Signals and Systems, Heriot-Watt University, Edinburgh, EH14 4AS, UK

Email: {xinwenliuyu, fengliuswjt}@163.com, {sunjian, zhangwsh}@sdu.edu.cn, cheng-xiang.wang@hw.ac.uk, p.fan@ieee.org

Abstract—This paper proposes 3D non-stationary multiple-input multiple-output (MIMO) geometry-based stochastic models (GBSMs) for high-speed train (HST) tunnel channels. Considering the line-of-sight (LoS), single-bounced (SB), and double-bounced (DB) components from the geometrical tunnel scattering model, a reference HST tunnel channel model under the assumption that scatterers are uniformly distributed on the tunnel walls is first derived. Then, by using the modified method of equal areas (MMEA), the corresponding simulation model is developed. Based on the proposed tunnel channel models, the correlation properties in time and space domains are investigated. A good agreement of statistical properties between the reference model and simulation model can be obtained. Furthermore, the simulation results show that the proposed model can be applied to mimic the non-stationarity of HST tunnel channels.

Index Terms—High-speed train, tunnel scenario, channel model, statistical properties.

I. INTRODUCTION

As a typical application scenario of fifth generation (5G) communications, HST wireless communication system has attracted more and more attentions recently [1]. Large numbers of HST users bring numerous communication data. Hence, new generation HST communication networks with high reliability are required [2]. Accurate channel models which can mimic the signal propagation are indispensable.

When the train travels on the track, it can encounter more than twelve HST scenarios, such as open space, viaduct, cutting, and tunnel [3]. Due to the confined space, rough interior tunnel walls, and waveguide effect, the signals propagation inside tunnels are quite different from those in other scenarios [4]. To acquire best performance of future HST tunnel communication systems, a comprehensive understanding of statistical properties of tunnel channel models is important [5]. Based on different modeling methods, a variety of tunnel channel models, such as ray tracing model [6], multi-mode model [7], [8], and geometrical-based model [9], were proposed and analyzed. In [6], the impact of different parameters on channel characteristics in a HST ray tracing tunnel channel model was investigated. The received power in different cases can be predicted. Combining the geometrical optical model and waveguide model, a multi-mode model for tunnel scenarios was proposed in [8]. The authors studied the received power at any location inside a tunnel. Most of the aforementioned works focus on large-scale fading, and ignore the small-scale fading characteristics. Based on the model proposed in [8], a

time-dependent multi-mode model was given [7], and some small-scale channel statistics were investigated. Moreover, a geometrical-based model for car-to-car tunnels was studied in [9]. It can describe the scattering environment using the geometry-based shape and investigate some small-scale fading characteristics. However, the proposed model is still a wide-sense stationary model. It can not mimic the non-stationarity resulting from fast movements of the transmitter (Tx) and/or receiver (Rx) accurately. In [10], a circular-like non-stationary tunnel channel model was proposed, and some small-scale fading characteristics were studied. However, it has too many parameters, which make the channel model more complex. To fill the research gap, novel 3D non-stationary MIMO geometry-based channel models with appropriate complexity in HST tunnel scenario are proposed, and some channel statistical properties are analyzed.

The reminder of this paper is organized as follows. In Section II, the geometrical tunnel scattering model is introduced. Based on this, 3D non-stationary HST tunnel channel models are proposed. Then, the corresponding correlation properties of proposed tunnel channel models are given in Section III. The simulation results and the analysis are presented in Section IV. Finally, conclusions are drawn in Section V.

II. 3D NON-STATIONARY HST TUNNEL CHANNEL MODELS

A MIMO HST tunnel communication system with P transmit and Q receive omni-directional antenna elements are considered. Based on this network architecture, an arched geometrical scattering model for HST tunnel channel is abstracted as shown in Fig. 1. When the train travels inside tunnels, the received signals are influenced by the arched internal surfaces of tunnel and the ground inside tunnel. This scattering model assumes that infinite number of scatterers are randomly distributed on the internal surfaces and ground, which follow the uniform distribution [9].

It is noted that the LoS and SB components carry more energy of signals propagating inside tunnels [10], DB components still carry some. Hence, based on the proposed scattering model, accurate HST tunnel channel models which combining the LoS, SB, and DB components are provided.

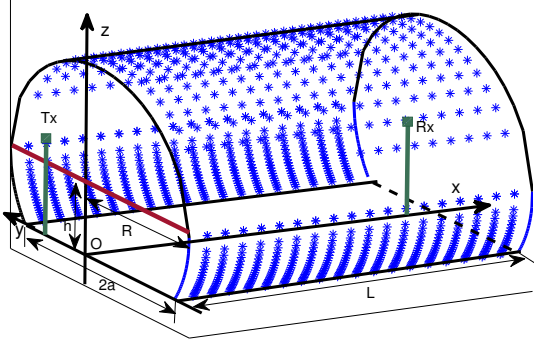


Fig. 1: Randomly distributed scatterers (*) on the arched tunnel surface with radius $R = 2.59$ m.

A. Reference Model

Considering the infinite number of scatterers randomly distributed on the tunnel surface, a 3D non-stationary reference tunnel channel model is proposed. The channel impulse response (CIR) between the p th antenna element of Tx and q th antenna element of Rx can be derived as

$$h_{pq}(t, \tau) = h_{pq}^{\text{LoS}}(t, \tau^{\text{LoS}}(t)) + \sum_k h_{pq}^{\text{SB}}(t, \tau_k^{\text{SB}}(t)) + \sum_l h_{pq}^{\text{DB}}(t, \tau_l^{\text{DB}}(t)) \quad (1)$$

where $h_{pq}^{\text{LoS}}(t, \tau^{\text{LoS}}(t))$, $h_{pq}^{\text{SB}}(t, \tau_k^{\text{SB}}(t))$, $h_{pq}^{\text{DB}}(t, \tau_l^{\text{DB}}(t))$ denote the impulse responses of the LoS, SB, and DB components, respectively.

In (1), the LoS component can be expressed as

$$h_{pq}^{\text{LoS}}(t) = \sqrt{\frac{K_{pq}}{K_{pq} + 1}} e^{-\frac{j2\pi D_{pq}(t)}{\lambda}} e^{j2\pi f_{R\max} t \cos(\alpha_{1,R}^{\text{LoS}}(t) - \varphi_R) \cos \beta_{1,R}^{\text{LoS}}} \quad (2)$$

where

$$D_{pq}(t) = \sqrt{(x_{pT} - x_{qR})^2 + (y_{pT} - y_{qR})^2 + (z_{pT} - z_{qR})^2} \quad (3)$$

and SB components can be expressed

$$h_{pq}^{\text{SB}}(t) = \lim_{M,N \rightarrow \infty} \frac{\eta_1}{\sqrt{(K_{pq} + 1)MN}} \sum_{m,n=1}^{M,N} e^{-\frac{j2\pi D_{1,pq}^{(m,n)}(t)}{\lambda}} e^{j2\pi f_{R\max} t \cos(\alpha_{1,R}^{(m,n)}(t) - \varphi_R) \cos \beta_{1,R}^{(m,n)}} \quad (4)$$

where

$$D_{1,pq}^{(m,n)}(t) = D_{1,pT}^{(m,n)}(t) + D_{1,qR}^{(m,n)}(t) \quad (5)$$

$$D_{1,pT}^{(m,n)}(t) = \sqrt{(x_{pT} - x_m)^2 + (y_{pT} - y_n)^2 + (z_{pT} - z_{mn})^2} \quad (6)$$

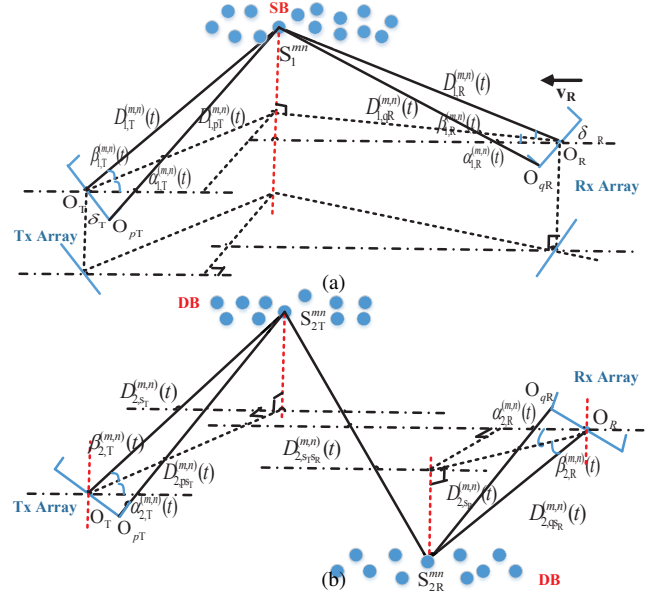


Fig. 2: Geometrical relationship of the SB and DB cases: (a) Time-varying angular parameters of the SB components of the HST tunnel channel model. (b) Time-varying angular parameters of the DB components of the HST tunnel channel model.

$$D_{1,qR}^{(m,n)}(t) = \sqrt{(x_{qR} - x_m)^2 + (y_{qR} - y_n)^2 + (z_{qR} - z_{mn})^2} \quad (7)$$

Here, the positions of the Tx and Rx are determined by (x_T, y_T, z_T) and (x_R, y_R, z_R) . The coordinates of the p th Tx antenna element and q th Rx antenna element are (x_{pT}, y_{pT}, z_{pT}) and (x_{qR}, y_{qR}, z_{qR}) , respectively. The positions of scatterers in the 3D space are presented as (x_m, y_n, z_{mn}) . For the arched tunnel part, $0 \leq x_m \leq L$, $-R \leq y_n \leq R$, and $z_{mn} = h + \sqrt{(R^2 - (y_n)^2)}$. For the ground part, $0 \leq x_m \leq L$, $-a \leq y_n \leq a$, and z_{mn} is constant. The width of ground part inside tunnel is $2a$, the radius of arched part is R , and the distance between the Tx and Rx is $L = x_R - v_R t - x_T$.

Using the trigonometric relationship in Fig. 2, the Azimuth AoA (AAoA) and Elevation AoA (EAoA) can be expressed as (8) and (9) for SB case, and the similar expressions can also be obtained in DB case. Moreover, there are:

$$\begin{cases} x_{pT} = x_T + k_p \cdot \delta_T \cdot \cos \varphi_T \cdot \cos \theta_T & (10) \\ y_{pT} = y_T + k_p \cdot \delta_T \cdot \cos \varphi_T \cdot \sin \theta_T & (11) \\ z_{pT} = z_T + k_p \cdot \delta_T \cdot \sin \varphi_T & (12) \end{cases}$$

$$\begin{cases} x_{qR} = x_R - v_R t + k_q \cdot \delta_R \cdot \cos \varphi_R \cdot \cos \theta_R & (13) \\ y_{qR} = y_R + k_q \cdot \delta_R \cdot \cos \varphi_R \cdot \sin \theta_R & (14) \\ z_{qR} = z_R + k_q \cdot \delta_R \cdot \sin \varphi_R & (15) \end{cases}$$

The DB components of tunnel can be expressed as

$$h_{pq}^{\text{DB}}(t) = \lim_{M,N \rightarrow \infty} \frac{\eta_2}{\sqrt{(K_{pq} + 1)MN}} \sum_{m,n=1}^{M,N} e^{-\frac{j2\pi D_{2,pq}^{(m,n)}(t)}{\lambda}} e^{j2\pi f_{R\max} t \cos(\alpha_{2,R}^{(m,n)}(t) - \varphi_R) \cos \beta_{2,R}^{(m,n)}} \quad (16)$$

where

$$D_{2,pq}^{(m,n)}(t) = D_{2,pT}^{(m,n)}(t) + D_{2,TR}^{(m,n)}(t) + D_{2,qR}^{(m,n)}(t) \quad (17)$$

$$\alpha_{1,R}^{(m,n)}(t) = \begin{cases} \pi - \arccos \frac{x_R - v_R t - x_m}{\sqrt{(x_m - x_R + v_R t)^2 + (y_n - y_R)^2}} & y_n > y_R \\ -\pi + \arccos \frac{x_R - v_R t - x_m}{\sqrt{(x_m - x_R + v_R t)^2 + (y_n - y_R)^2}} & y_n < y_R \end{cases} \quad (8)$$

$$\beta_{1,R}^{(m,n)}(t) = \begin{cases} \pi - \arccos \frac{\sqrt{(x_m - x_R + v_R t)^2 + (y_n - y_R)^2}}{\sqrt{(x_m - x_R + v_R t)^2 + (y_n - y_R)^2 + (z_{mn} - z_R)^2}} & z_{mn} > z_R \\ -\pi + \arccos \frac{\sqrt{(x_m - x_R + v_R t)^2 + (y_n - y_R)^2}}{\sqrt{(x_m - x_R + v_R t)^2 + (y_n - y_R)^2 + (z_{mn} - z_R)^2}} & z_{mn} < z_R \end{cases} \quad (9)$$

$$D_{2,pT}^{(m,n)}(t) = \sqrt{(x_{pT} - x_{mT})^2 + (y_{pT} - y_{nT})^2 + (z_{pT} - z_{mnT})^2} \quad (18)$$

$$D_{2,qR}^{(m,n)}(t) = \sqrt{(x_{qR} - x_{mR})^2 + (y_{qR} - y_{nR})^2 + (z_{qR} - z_{mnR})^2} \quad (19)$$

$$D_{2,TR}^{(m,n)}(t) = \sqrt{(x_{pT} - x_{qR})^2 + (y_{pT} - y_{qR})^2 + (z_{mnT} - z_{mnR})^2}. \quad (20)$$

Here, the positions of scatterers near the Tx and Rx can be denoted by $(x_{mT}, y_{nT}, z_{mnT})$, $(x_{mR}, y_{nR}, z_{mnR})$, respectively. There are $0 \leq x_{mT} \leq L/2$ and $L/2 \leq x_{mR} \leq L$. For the arched tunnel part, it has $-R \leq y_{nR}/n_T \leq R$ and $z_{mnT}/mnR = h + \sqrt{R^2 - (y_{nT}/n_R)^2}$. For the ground part, $-a \leq y_{nR}/n_T \leq a$, and z_{mnT}/mnR is constant. The received signals can be obtained by the summation of LoS, SB, and DB components, and the total power of these three parts can be kept as 1. η_1 is the power percentage in SB, and η_2 is in DB case. All the related parameters in Fig. 2 can be listed as follows

TABLE I: Definition of parameters.

Parameters	Definition
$D_{1,pT}^{(m,n)}(t), D_{1,qR}^{(m,n)}(t)$	the distance $d(O_{pT}, S_1^{mn})$ and $d(S_1^{mn}, O_{qR})$
$D_{2,psT}^{(m,n)}(t), D_{2,qsR}^{(m,n)}(t)$	the distance $d(O_{pT}, S_2^{mn})$ and $d(S_2^{mn}, O_{pT})$
$D_{2,TR}^{(m,n)}(t)$	the distance $d(S_2^{mn}, S_2^{mn})$
$\alpha_{1,T}^{(m,n)}(t), \beta_{1,T}^{(m,n)}(t)$	the AAoD and EAoD in SB case
$\alpha_{1,R}^{(m,n)}(t), \beta_{1,R}^{(m,n)}(t)$	the AAoA and EAoA in SB case
$\alpha_{2,T}^{(m,n)}(t), \beta_{2,T}^{(m,n)}(t)$	the AAoD and EAoD in DB case
$\alpha_{2,R}^{(m,n)}(t), \beta_{2,R}^{(m,n)}(t)$	the AAoA and EAoA in DB case
δ_T, δ_R	the antenna elements spacings of Tx and Rx
φ_T, φ_R	the azimuth angles of Tx and Rx antenna
θ_T, θ_R	the elevation angles of Tx and Rx antenna
v_R	the moving speed of Rx

B. Simulation Model

In the reference model, an infinite number of scatterers are assumed on the tunnel surface, which can not be used in the

real simulations. Hence, based on the above reference tunnel channel model, the corresponding simulation model can be developed. According to (1), the simulation for the link from p th Tx element to q th Rx element can be expressed as

$$\tilde{h}_{pq}(t, \tau) = \tilde{h}_{pq}^{\text{LoS}}(t, \tau^{\text{LoS}}(t)) + \sum_k \tilde{h}_{pq}^{\text{SB}}(t, \tau_k^{\text{SB}}(t)) + \sum_l \tilde{h}_{pq}^{\text{DB}}(t, \tau_l^{\text{DB}}(t)). \quad (21)$$

From the reference model to the simulation model, it is a discretization process of continuous random distribution. The simulation model is obtained by discrete values x_m, y_n in SB case and x_{mR}, y_{nR} in DB case. To calculate the above discrete values accurately, the MMEA method is used as the expression (37) in [11]. The remain parameters are same to those in reference model.

III. CORRELATION PROPERTIES OF PROPOSED TUNNEL CHANNEL MODELS

In this section, some important channel statistical properties of the proposed channel models, such as the cross-correlation function (CCF) and the autocorrelation function (ACF), are derived. The correlation of two CIRs $h_{pq}(t)$ and $h_{p'q'}^*(t - \Delta t)$ can be expressed as follows

$$R_h(t, \delta_T, \delta_R, \Delta t) = E[h_{pq}(t) \cdot h_{p'q'}^*(t - \Delta t)] \quad (22)$$

where $(\cdot)^*$ stands for the conjugate operation, and $E[\cdot]$ denotes the expectation operator.

A. CCF

According to (22), the time-variant space CCF can be acquired by imposing $\Delta_T = 0$, which is further expressed as

$$\rho_h(t, \delta_T, \delta_R) = R_h(t, \delta_T, \delta_R, 0) = \rho_h^{\text{LoS}}(t, \delta_T, \delta_R) + \rho_h^{\text{SB}}(t, \delta_T, \delta_R) + \rho_h^{\text{DB}}(t, \delta_T, \delta_R) \quad (23)$$

– In the case of LoS,

$$\rho_h^{\text{LoS}}(t, \delta_T, \delta_R) = \frac{K_{pq}}{K_{pq} + 1} e^{j2\pi \frac{D_{p'q'}(t) - D_{pq}(t)}{\lambda}} \quad (24)$$

– In the case of SB,

$$\rho_h^{\text{SB}}(t, \delta_T, \delta_R) = \frac{\eta_1}{(K_{pq}+1)LW} \int_{x_T}^{x_R} \int_0^W e^{j2\pi \frac{D_{1,p'q'}^{(m,n)} - D_{1,pq}^{(m,n)}}{\lambda}} dx_m dy_n \quad (25)$$

– In the case of DB,

$$\rho_h^{\text{DB}}(t, \delta_T, \delta_R) = \frac{\eta_2}{(K_{pq}+1)LW} \int_{x_T}^{x_R} \int_0^W e^{j2\pi \frac{D_{2,p'q'}^{(m,n)} - D_{2,pq}^{(m,n)}}{\lambda}} dx_m dy_n. \quad (26)$$

B. ACF

By imposing $\delta_T = 0$ and $\delta_R = 0$, the time-variant ACFs can be obtained as follows

$$r_h(t, \Delta t) = R_h(t, 0, 0, \Delta t) = r_h^{\text{LoS}}(t, \Delta t) + r_h^{\text{SB}}(t, \Delta t) + r_h^{\text{DB}}(t, \Delta t) \quad (27)$$

– In the case of LoS,

$$r_h^{\text{LoS}}(t, \Delta t) = \frac{K_{pq}}{K_{pq} + 1} e^{j2\pi f_{R\max} \Delta t \cos \alpha_R^{\text{LoS}}(t) \cos \beta_R^{\text{LoS}}(t)} \quad (28)$$

– In the case of SB,

$$r_h^{\text{SB}}(t, \Delta t) = \frac{\eta_1}{(K_{pq}+1)(LW)MN} \int_{x_T}^{x_R} \int_0^W e^{j2\pi f_{R\max} \Delta t \cos \alpha_{1,R}^{(m,n)}(t) \cos \beta_{1,R}^{(m,n)}(t)} dx_m dy_n \quad (29)$$

– In the case of DB,

$$r_h^{\text{DB}}(t, \Delta t) = \frac{\eta_2}{(K_{pq}+1)((x_R - v_R t - x_T)W)MN} \int_{x_T}^{x_R} \int_0^W e^{j2\pi f_{R\max} \Delta t \cos \alpha_{2,R}^{(m,n)}(t) \cos \beta_{2,R}^{(m,n)}(t)} dx_m dy_n. \quad (30)$$

IV. SIMULATION RESULTS AND THE ANALYSIS

In this section, the correlation properties of proposed tunnel channel models are analyzed. Here, we consider the arched tunnel and ground parts to do some derivations and simulations. The initial coordinates of Tx and Rx are $(x_T, y_T, z_T) = (0, 1.79, 3)$ and $(x_R, y_R, z_R) = (150, 0, 3)$, respectively. Moreover, the carrier frequency $f_c = 5.7$ GHz, the Doppler spread $f_{R\max} = 1900$ Hz, the LoS Ricean factor $K_{pq} = 20$ dB, and the initial propagation distance is 150 m [12]. The number of scatterers can be applied for the simulation model to describe the statistical properties of channel model, is selected as $M \times N = 50 \times 50$.

A. CCF

By adopting the antenna element spacing at Tx $\delta_T = \lambda$, the absolute values of the 3D space CCF are illustrated as Fig. 3. From this figure, we can easily observe that the space CCF decreases as the antennas element spacing δ_R increases. Moreover, Fig. 3 also shows the absolute values of the time-variant CCFs at different time instants. We can notice that the absolute values of space CCF change with time t due to the non-stationary propagation channel.

Fig. 4 shows a comparison between the time-variant space CCF of reference tunnel channel model and the simulation model at different time instants $t = 0$ s, 0.5 s and 1 s. It presents that the simulation model can approximate the reference model very well.

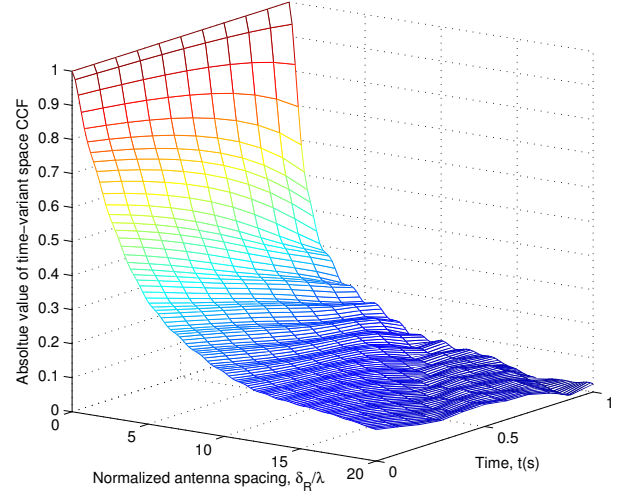


Fig. 3: Absolute values of space CCFs of 3D tunnel channel model ($v_R = 360$ km/h, $f_c = 5.7$ GHz).

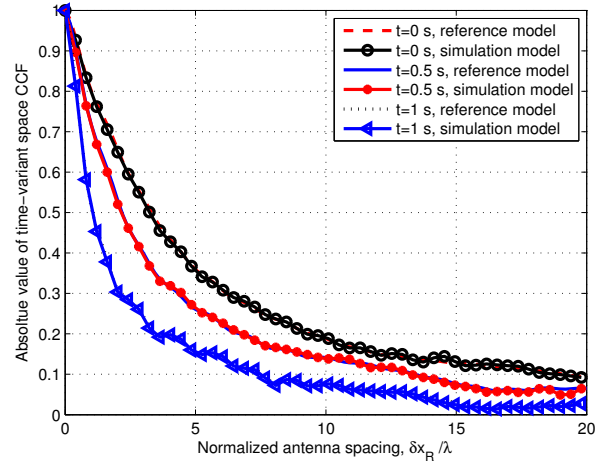


Fig. 4: Comparison between the space CCFs of reference model and simulation model at different time instants ($v_R = 360$ km/h, $f_c = 5.7$ GHz).

B. ACF

By adopting the antenna element spacings $\delta_T = \lambda$ and $\delta_R = \lambda$ in (27), the absolute values of 3D time ACF are given in Fig. 5. From this figure, we can notice that the ACF decreases with time difference Δt increases. Furthermore, due to the non-stationarity of channel, the absolute values of ACFs in different time instants t have different variation trends.

Fig. 6 illustrates the absolute values of time-variant ACFs with and without LoS component. From this figure, we can easily observe that the ACF has the higher correlation when considering the LoS component comparing with that case without LoS component.

Fig. 7 shows the comparison between the time-variant ACF of reference model and simulation model. The ACFs have different variation trends at different time instants, i.e., $t = 0$ s, 0.5 s, 1 s, respectively. Furthermore, the ACFs of simulation model can provide a good approximation of reference model.

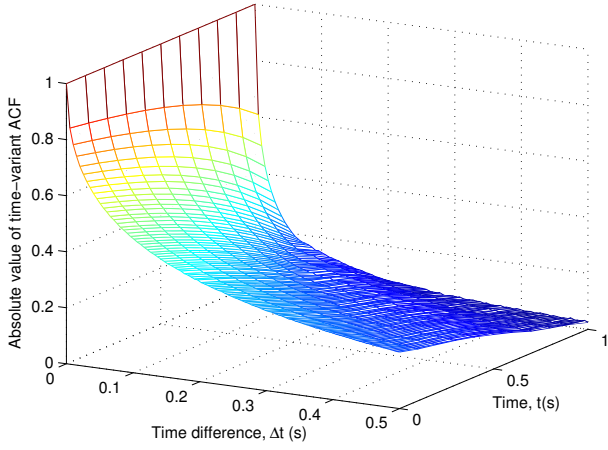


Fig. 5: Absolute values of space ACFs of 3D tunnel channel model

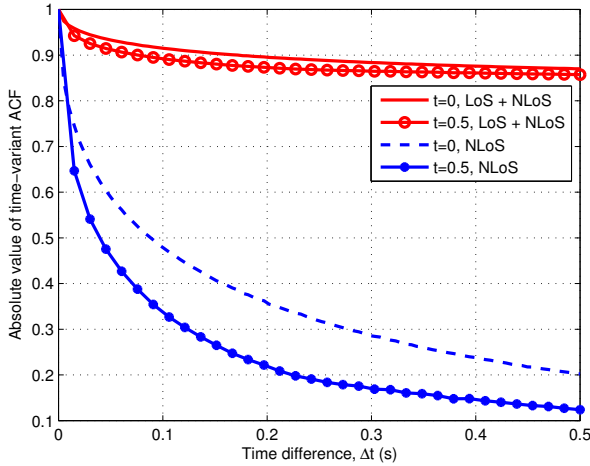


Fig. 6: Absolute values of the time-variant ACFs of the simulation model with and without the LoS component at different time instants ($v_R = 360$ km/h, $f_c = 5.7$ GHz, $K_{pq} = 20$ dB).

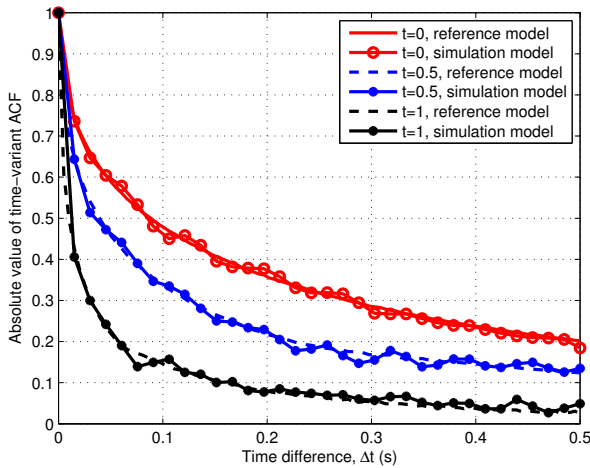


Fig. 7: Comparison between the time ACFs of the reference model and simulation model with time-variant angles at different time instants ($v_R = 360$ km/h, $f_c = 5.7$ GHz).

V. CONCLUSION

In this paper, a 3D reference non-stationary MIMO GBSM for HST tunnel channels has been proposed. By using the

MMEA method, a corresponding simulation model has been developed. The proposed models have appropriate complexity, which are just related to the real size of tunnel scenario, such as the tunnel width, tunnel length and tunnel radius. The statistical properties of the simulation model can provide good approximations of the reference model. Moreover, the time-variant statistical properties, such as the space CCF and time ACF, have been investigated, which can describe the non-stationary tunnel channels well. The numerical results have shown that the ACFs and CCFs have different behaviors at different time instants, demonstrating that the proposed model has the capacity to describe the non-stationarity of HST tunnel channels. In the future work, we will consider more channel characteristics based on the proposed HST tunnel model, and carry on some comparison with the current similar models.

ACKNOWLEDGMENT

The authors would like to acknowledge the support from the Natural Science Foundation of China (Grant No. 61771293), EU H2020 ITN 5G Wireless project (Grant No. 641985), EU H2020 RISE TESTBED project (Grant No. 734325), Key R&D Program of Shandong Province (Grant No. 2016GGX101014), Fundamental Research Funds of Shandong University (Grant No. 2017JC029), China Postdoctoral Science Foundation Funded Project (Grant No. 2017M622203), and National Postdoctoral Program for Innovative Talents (Grant No. BX201700308).

REFERENCES

- [1] C.-X. Wang, A. Ghazal, B. Ai, P. Fan, and Y. Liu, "Channel measurements and models for high-speed train communication systems: a survey," *IEEE Commun. Surveys Tut.*, vol. 18, no. 2, pp. 974-987, 2nd Quart., 2016.
- [2] X. Ge, S. Tu, G. Mao, C.-X. Wang, and T. Han, "5G ultra-dense cellular networks," *IEEE Wireless Commun.*, vol. 23, no. 1, pp. 72-79, Feb. 2016.
- [3] B. Ai, R. He, Z. Zhong, K. Guan, B. Chen, P. Liu, and Y. Li, "Radio wave propagation scene partitioning for high-speed rails," *Int. J. Antennas Propag.*, vol. 2012, Article ID 815232, 7 pages, 2012.
- [4] K. Guan, Z.D. Zhong, B. Ai, R.S. He, B.H. Chen, Y. X. Li, and C. Briso, "Complete Propagation Modeling in Tunnels," *IEEE Antennas and Wireless Propag. Letters*, vol. 12, pp. 741-744, 2013.
- [5] Y. Liu, A. Ghazal, C.-X. Wang, X. Ge, Y. Yang, and Y. Zhang, "Channel measurements and models for high-speed train wireless communication systems in tunnel scenarios: a survey," *Sci. China Inf. Sci.*, vol. 60, no. 8, Oct. 2017.
- [6] Y. Zhang, Y. Liu, J. Sun, C.-X. Wang, and X. Ge, "Impact of different parameters on channel characteristics in a high-speed train ray tracing tunnel channel model," in *Proc. IEEE VTC17-Spring*, Sydney, Australia, June 2017.
- [7] Y. Liu, C.-X. Wang, A. Ghazal, S. Wu, and W. Zhang, "A multi-mode waveguide tunnel channel model for high-speed train wireless communication systems," in *Proc. EuCAP15*, Lisbon, Portugal, Apr. 2015.
- [8] Z. Sun and I. F. Akyildiz, "Channel modeling and analysis for wireless networks in underground mines and road tunnels," *IEEE Trans. Commun.*, vol. 58, no. 6, pp. 17581768, June 2010.
- [9] N. Avazov and M. Patzold, "A novel wideband MIMO car-to-car channel model based on a geometrical semi-circular tunnel scattering model," *IEEE Trans. Veh. Technol.*, vol. 65, no. 3, pp. 10701082, Mar. 2016.
- [10] Y. Liu, C.-X. Wang, C. F. Lopez, and X. Ge, "3D non-stationary wideband tunnel channel models for high-speed train wireless communication systems," *Sci. China Inf. Sci.*, vol. 60, no. 8, Aug. 2017.
- [11] A. Ghazal, C.-X. Wang, B. Ai, D. Yuan, and H. Haas, "A non-stationary wideband MIMO channel model for high-mobility intelligent transportation systems," *IEEE Trans. Intell. Transp. Syst.*, vol. 16, no. 2, pp. 885-897, Apr. 2015.
- [12] J. X. Li, Y. P. Zhao, J. Zhang, R. Jiang, C. Tao, Z. H. Tan, "Radio channel measurements and analysis at 2.4/5GHz in subway tunnels," *China Commun.*, vol. 12, no. 1, pp. 36C45, Jan. 2015.